Micro-statics and micro-kinematics of capillary phenomena in dense granular materials

B. Chareyre, L. Scholtès and F. Darve

Laboratoire 3S-R, Domaine Universitaire BP 53, 38041 Grenoble cedex 9, France

Abstract. A capillary stress tensor and an effective stress tensor are defined in DEM simulations of spheres packings with capillary effect. It is shown that induced fabric anisotropy results in an anisotropy of the capillary stress, so that any stress-like variable used to represent the effect of capillarity in granular materials should be represented by a non-spherical tensor. The response of a sample to small isotropic stress increments is also presented, the loading being imposed either by a small variation of the stress imposed at boundaries (method A) or by a variation of matric suction (method B). The comparison of the results, with emphasis on micromechanical aspects, shows some differences between the results obtained with methods A and B, even though the increment of effective stress is the same in both cases. The effective stress concept in unsaturated granular materials is questionned on the basis of these results.

Keywords: micromechanics; granular materials; unsaturated; DEM; capillary forces; microstructure
PACS: <Replace this text with PACS numbers; choose from this list: `http://www.aip..org/pacs/index.html`>

INTRODUCTION

Macroscopic properties of granular materials such as soils depend on particle interactions. In unsaturated soils submitted to capillary effects, the presence of water leads to the formation of water menisci between neighboring grains, introducing new interparticle forces at contact. For low water contents, water is under the form of liquid bridges between grains, capillary theory allows the force induced by those bridges to be linked to the local geometry of the grains and to the capillary pressure inside the medium. Along these lines we developped a micromechanical model based on the Discrete Element Method [1], which takes into account capillary forces between grains. Simulations are carried out on grain assemblies whose response to different loading paths are related to some microscale kinematic and static variables. Investigating those variables offer an insight into the debated unsaturated soil stress framework.

Stresses in unsaturated granular materials - macroscopic views

In the framework of elastoplasticity, most models consider that the strain tensor is governed by the net stress tensor $\sigma_{ij} - u_a\delta_{ij}$ (u_a being the pore air pressure) and the matric suction or capillary pressure $u_a - u_w$ (u_w being the pore water pressure) inside the medium [3**?** , 2]. All these formulations can be considered as extensions of the relationship initially proposed by Bishop and Blight [4] for unsaturated soils:

$$\sigma'_{ij} = (\sigma_{ij} - u_a\delta_{ij}) + \chi(S_r)(u_a - u_w)\delta_{ij} \qquad (1)$$

where $\chi(S_r)$ is called the effective stress parameter or Bishop's parameter, and is a function of the degree of saturation S_r of the medium. Despite the effective stress principle is by definition a macroscopic concept, several authors (Lu and Likos [5] or Li [6]) proposed to use a micromechanical approach for the effective stress principle. Such approach is proposed in the followings, based on a set of simulated laboratory experiments.

A micromechanical interpretation

A simple expression relating the overall stress tensor in such packing to the force distribution can be derived using the Love [7] static homogenisation relation. Love relation reads:

$$\sigma_{ij} = \frac{1}{V}\sum_{p=1}^{N}\sum_{q=1}^{N} F_i^{q,p} l_j^{q,p} \qquad (2)$$

where N is the number of particles within the volume, $\vec{F}^{q,p}$ is the interaction force exerted by the particle q onto the particle p, and $\vec{l}^{q,p}$ is the branch vector pointing from particle q to particle p ($\vec{l}^{q,p} = \vec{x}^p - \vec{x}^q$). The expression of Eq. (3), as proposed in [8], is a generalization of Love relation for wet granular materials, considering that interaction forces as the sum of a solid ($F_{cont,i}$, repulsive) and capillary ($F_{cap,i}$, attractive) forces. On this basis, the total stress can be split into two components as in Eq. (4).

$$\sigma_{ij} = \frac{1}{V}\sum_{p=1}^{N}\sum_{q=1}^{N} F_{cont,i}^{q,p} l_j^{q,p} + \frac{1}{V}\sum_{p=1}^{N}\sum_{q=1}^{N} F_{cap,i}^{q,p} l_j^{q,p} \qquad (3)$$

$$\sigma_{ij} = \sigma_{ij}^{cont} + \sigma_{ij}^{cap} \qquad (4)$$

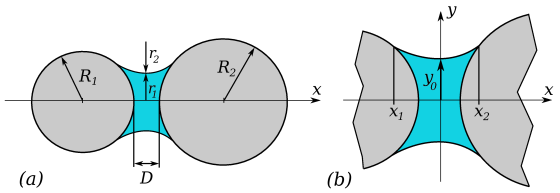

FIGURE 1. Liquid bridge between two particles of unequal sizes: (a) global geometry, (b) details of the bridge.

the contact stress tensor σ_{ij}^{cont} accounting for the contact forces transmitted along the contact network, and the capillary stress tensor σ_{ij}^{cap} representing the effect of capillary forces existing within the assembly. Considering the concept as initially introduced by Terzaghi, σ_{ij}^{cont} can play the role of the so-called effective stress by governing soil deformation and failure. By analogy with Eq.(1), Scholtes et al. [9] proposed to used it as a definition of a microstructural effective stress.

DISCRETE ELEMENT MODELLING

A numerical model of capillary forces has been developed and implemented in the 3D open source code YADE (see Kozicki and Donzé [10]), which is based on the discrete element method as initially introduced by Cundall and Strack [1].

The solid contact interaction is described by an elastic-plastic relation between the force F and the relative displacement U of two interacting particles. The parameters of the relation are the normal stiffness K_n, the tangential stiffness K_t, and the intergranular friction angle ϕ.

We assume that the water inside the sample is only composed of capillary water as defined in the pendular state, with disconnected liquid bridges between grains (see Fig. 1). The exact shape of liquid bridges is defined by the Laplace equation, relating the pressure jump $\Delta u = u_a - u_w$ across the liquid-gas interface to the mean curvature of the bridge and the surface tension of the liquid phase γ as :

$$\Delta u = \gamma \left(\frac{1}{r_1} + \frac{1}{r_2} \right) \tag{5}$$

This equation has been solved numerically, for the case of spheres of different sizes, in order to link directly the suction Δu to the capillary force F_{cap} and water volume V of the liquid bridge bewtween grains [8]. This approach results in a suction-controlled model where capillary forces and water volumes (F_{cap}, V) are functions of the imposed suction level Δu.

The studied particle assembly is a 1 mm length cubic sample of 10000 spheres, with a grain size distribution ranging from $0.025\,mm$ to $0.08\,mm$, and a porosity of 0.385. The parameters of contact laws are $K_n = 300.\frac{R1+R2}{R1R2}$ (MN/m), $K_t = 0.5.K_n$, and $\phi = 30$.

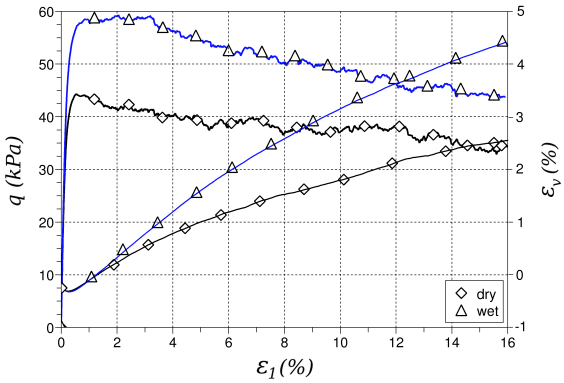

FIGURE 2. stress-strain curves in triaxial compression tests simulated at constant on a dry and wet samples (suction of $20\,kPa$ and confinement pressure $30\,kPa$.

Random packings are prepared by a compaction technique which ensures the packing isotropy and homogeneity [8]. Loose samples can be obtained if suction is activated during the compaction phase. Suction-controlled triaxial loadings are simulated on the generated specimens. Two types of loadings are presented in this paper : constant suction / variable external stress (referenced later as type A), and variable suction / constant external stress (type B). For type A, the imposed stress-strain paths are either deviatoric (constant strain rate imposed in one direction and constant stress in other directions) or isotropic (all three principal stresses are imposed).

RESULTS

Macroscopic views

Fig. 2 shows the evolution of the deviatoric stress versus the axial strain in a type-A deviatoric loading path for a dense sample in a dry and a wet configuration respectively. The shear strength of the material is clearly increased by the presence of capillary forces. Fig. 3 shows the evolution of the principal capillary stress components during the loading. It is to be noted that the capillary stress varies during the loading, even though the imposed suction itself is constant, and also that an anisotropy develops with the deformation.

Fig. 4 presents the volumetric deformation produced by a cyclic loading of type B on a loose sample under a constant and isotropic external stress. The stress is given in terms of contact stress. The results show a volumetric

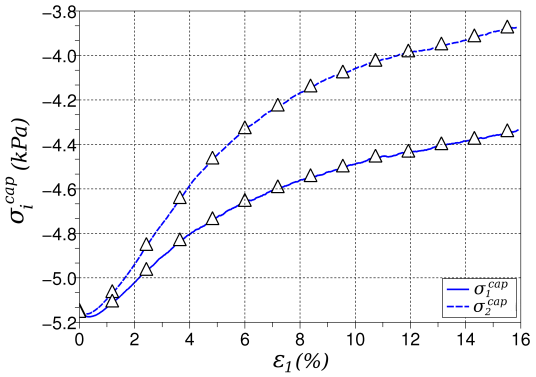

FIGURE 3. Evolution of capillary stress components in triaxial tests simulated at constant suction

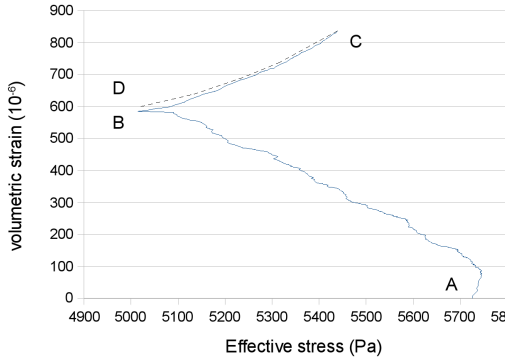

FIGURE 4. Volumetric strain versus contact stress in a cyclic capillary loading : imbibition (A-B), drainage (B-C), imbibition (C-D). A positive value is a compression.

collapse induced by the first wetting cycle A-B (Δu from $30kPa$ to $10kPa$), and a reversible behaviour for the following cycles B-C and C-D.

Starting from state D, small stress increments of both types are imposed and reported on Fig. 5. The responses are reversible and can be considered in the elastic regime, but it has to be noted that the stress/strain relation (the effective stiffness) is not the same for increments of types A and B.

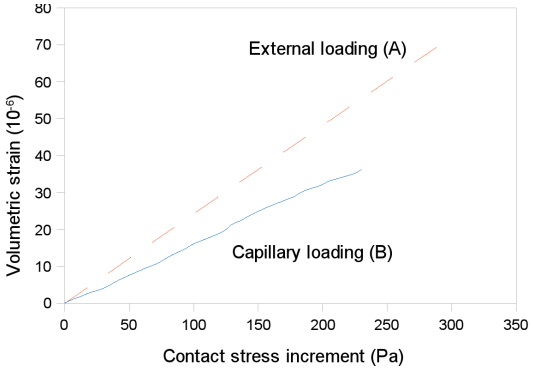

FIGURE 5. Volumetric response to small stress increments with loading types A and B.

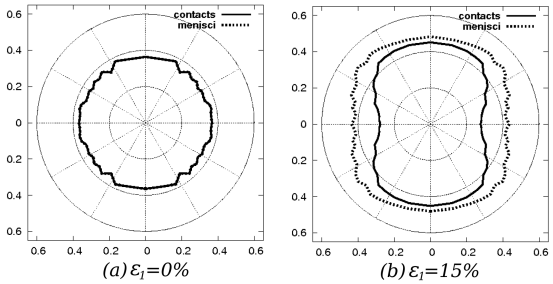

FIGURE 6. Contacts and menisci orientation distribution $P(\vec{n})$: (a) initial state, (b) 15% deformation level.

Micromechanical investigations

The distributions of the orientations of both contacts and meniscii during the triaxial loading (Fig. 2) are plotted on Fig.6, where θ corresponds to the angle of the unit normal vector $(\vec{n})$ from the axis of axisymmetry of the sample. Both contacts and menisci distributions are identical in the initial state. The structural isotropy of the sample appears clearly with a uniform distribution along all the directions (Figs.6(a)), confirming here the accuracy of the generation process. However, after a 15% deformation level, the distributions are anisoropic. As liquid bridges can exist in a certain range of increasing intergranular distances, the distribution of liquid bridges does not exactly follow the evolution of contacts network, and tends to stay closer to the initial state. But due to the sample dilatancy, a small induced anisotropy arises from the disappearance of liquid bridges in the lateral directions (Figs.6(b)).

The distribution of the normal displacement at contacts in the two increments of Fig. 5 are plotted and compared in Fig. 7. The displacements dU_n^* is normalised, so that we would have $dU_n^* = 1$, for all contacts, if the relative displacement between two grains was always exactly $\varepsilon_{ij}.l_j$ (l_j is the branch vector linking the centers of grains). Clear differences between the ditributions can be seen. For an external loading, the distribution is almost symetric, with a spreading of dU_n around one unique value. With a capillary loading, on the other hand, the ditribution has two peaks, one is close to 0 and the other one is around 5, which suggests that there are two different groups of contacts, or two types of mechanisms acting at the local scale, with each of them corresponding to one of the peak values.

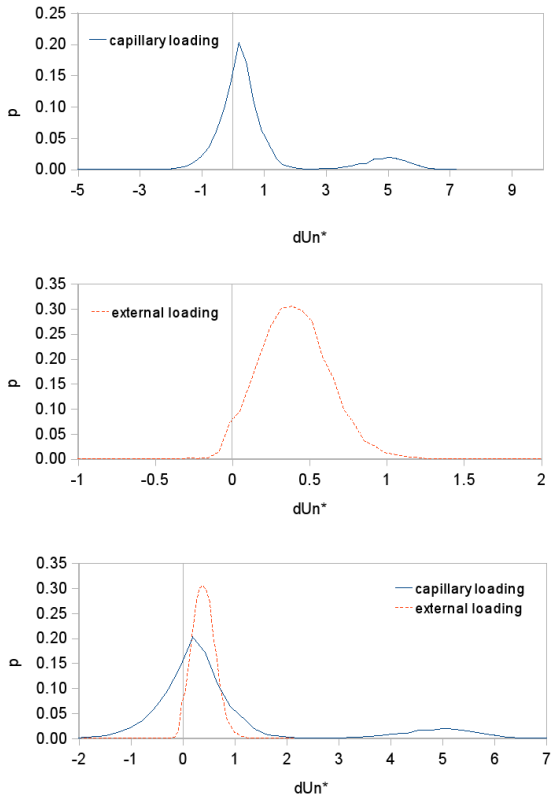

FIGURE 7. Distribution of normal displacement at contacts for stress increments : (a) capillary loading, (b) external loading, (c) comparison.

DISCUSSION

The results lead to some questions about the stresses induced by capillarity. Indeed, suction effects are classicaly viewed as an equivalent pressure which isotropic (see Eq.(1)) and also independant on the history of the loading. As seen in Fig.3, computing the principal components of this capillary stress tensor along the deviatoric loading path of a triaxial test compromises both assumptions.

As seen in section 2.2, σ_{ij}^{cap} can be written as:

$$\sigma_{ij}^{cap} = \frac{1}{V}\sum_{p=1}^{N}\sum_{q=1}^{N} F_{cap}^{q,p} l^{q,p} n_i^{p,q} n_j^{p,q} \qquad (6)$$

or, putting it in the continuous integral form with $P_{meniscus}(\vec{n})$ the normal density of menisci in the direction $\vec{n}$:

$$\sigma_{ij}^{cap} = \frac{1}{V}\int_V < F_{cap}.l >_{\vec{n}} P_{meniscus}(\vec{n})\vec{n}\otimes\vec{n}dV \qquad (7)$$

which clearly points out the origin of the evolution and anisotropy of σ_{ij}^{cap} is the anisotropy in the interaction network, induced by the deformation. It suggests that the pore fluid in unsaturated soil has its own fabric that may be readily altered with changes in the granular fabric. The global approximation which characterizes water effects in unsaturated materials by an equivalent pore pressure is, therefore, unable in essence to point out this intrinsically anisotropic microstructural force contribution.

The non-uniqueness of the relation between σ^{cont} and the deformation of the sample, as seen in Fig. 5, is another remarkable result of the simulations. The same increment in σ^{cap} will give different responses of the material depending on the origin of the applied stress, which seems to be in contradiction with the effective stress concept itself. This result is supported, and partly explained by the result of Fig. 7, which prooves that the deformation mechanisms are qualitatively different at the microscale. More investigations are needed to fully understand the reasons for these differences, and the DEM is a promising way for such research.

REFERENCES

1. Cundall PA, Strack ODL. A discrete numerical model for granular assemblies. *Géotechnique* 1979; **29**(1):47-65.
2. Nuth M, Laloui L. Effective stress concept in unsaturated soils: clarification and validation of a unified framework. *Int. Journal for Numerical and Analytical Methods in Geomechanics* 2008; **32**:771-801.
3. Alonso EE, Gens A, Hight DW. A constitutive model for partially saturated soils. *Géotechnique* 1990; **40**(3):405-430.
4. Bishop AW, Blight GE. Somme aspects of effective stress in saturated and partly saturated soils. *Géotechnique* 1963; **13**(3):177-197.
5. Lu N, Likos WJ. Suction stress characteristic curve for unsaturated soil. *J. of Geotechnical and Geoenvironmental Engineering* 2006; **132**(2):1090-0241.
6. Li XS. Effective stress in unsaturated soil: A microstructural analysis. *Géotechnique* 2003; **53**:273-277.
7. Love AEH. *A treatise on the mathematical theory of elasticity*. Cambridge University Press, Cambridge, 1927.
8. Scholtès L, Hicher P-Y, Nicot F, Chareyre B, Darve F. On the capillary stress tensor in wet granular materials. *Int. J. for Numerical and Analytical Methods in Geomechanics* 2008; DOI:10.1002/nag.767.
9. Scholtès L, Chareyre B, Nicot F, Darve F. Micromechanics of granular materials with capillary effects. *Int. J. of Engineering Science* 2008; DOI:.
10. Kozicki J, Donze FV. A new open-source software using a discrete element method to simulate granular material. *Computer Methods in Applied Mechanics and Engineering* 2008; **197**:4429-4443.